

Search for  $\eta$  and  $\eta'$  Invisible Decays in  $J/\psi \rightarrow \phi\eta$  and  $\phi\eta'$ 

M. Ablikim<sup>1</sup>, M. N. Achasov<sup>5</sup>, O. Albayrak<sup>3</sup>, D. J. Ambrose<sup>39</sup>, F. F. An<sup>1</sup>, Q. An<sup>40</sup>, J. Z. Bai<sup>1</sup>, Y. Ban<sup>27</sup>, J. Becker<sup>2</sup>, J. V. Bennett<sup>17</sup>, M. Bertani<sup>18A</sup>, J. M. Bian<sup>38</sup>, E. Boger<sup>20,a</sup>, O. Bondarenko<sup>21</sup>, I. Boyko<sup>20</sup>, R. A. Briere<sup>3</sup>, V. Bytev<sup>20</sup>, X. Cai<sup>1</sup>, O. Cakir<sup>35A</sup>, A. Calcaterra<sup>18A</sup>, G. F. Cao<sup>1</sup>, S. A. Cetin<sup>35B</sup>, J. F. Chang<sup>1</sup>, G. Chelkov<sup>20,a</sup>, G. Chen<sup>1</sup>, H. S. Chen<sup>1</sup>, J. C. Chen<sup>1</sup>, M. L. Chen<sup>1</sup>, S. J. Chen<sup>25</sup>, Y. B. Chen<sup>1</sup>, H. P. Cheng<sup>14</sup>, Y. P. Chu<sup>1</sup>, D. Cronin-Hennessy<sup>38</sup>, H. L. Dai<sup>1</sup>, J. P. Dai<sup>1</sup>, D. Dedovich<sup>20</sup>, Z. Y. Deng<sup>1</sup>, A. Denig<sup>19</sup>, I. Denysenko<sup>20,b</sup>, M. Destefanis<sup>43A,43C</sup>, W. M. Ding<sup>29</sup>, Y. Ding<sup>23</sup>, L. Y. Dong<sup>1</sup>, M. Y. Dong<sup>1</sup>, S. X. Du<sup>46</sup>, J. Fang<sup>1</sup>, S. S. Fang<sup>1</sup>, L. Fava<sup>43B,43C</sup>, F. Feldbauer<sup>2</sup>, C. Q. Feng<sup>40</sup>, R. B. Ferrolri<sup>18A</sup>, C. D. Fu<sup>1</sup>, J. L. Fu<sup>25</sup>, Y. Gao<sup>34</sup>, C. Geng<sup>40</sup>, K. Goetzen<sup>7</sup>, W. X. Gong<sup>1</sup>, W. Gradl<sup>19</sup>, M. Greco<sup>43A,43C</sup>, M. H. Gu<sup>1</sup>, Y. T. Gu<sup>9</sup>, Y. H. Guan<sup>6</sup>, A. Q. Guo<sup>26</sup>, L. B. Guo<sup>24</sup>, Y. P. Guo<sup>26</sup>, Y. L. Han<sup>1</sup>, F. A. Harris<sup>37</sup>, K. L. He<sup>1</sup>, M. He<sup>1</sup>, Z. Y. He<sup>26</sup>, T. Held<sup>2</sup>, Y. K. Heng<sup>1</sup>, Z. L. Hou<sup>1</sup>, H. M. Hu<sup>1</sup>, T. Hu<sup>1</sup>, G. M. Huang<sup>15</sup>, G. S. Huang<sup>40</sup>, J. S. Huang<sup>12</sup>, X. T. Huang<sup>29</sup>, Y. P. Huang<sup>1</sup>, T. Hussain<sup>42</sup>, C. S. Ji<sup>40</sup>, Q. Ji<sup>1</sup>, Q. P. Ji<sup>26,c</sup>, X. B. Ji<sup>1</sup>, X. L. Ji<sup>1</sup>, L. L. Jiang<sup>1</sup>, X. S. Jiang<sup>1</sup>, J. B. Jiao<sup>29</sup>, Z. Jiao<sup>14</sup>, D. P. Jin<sup>1</sup>, S. Jin<sup>1</sup>, F. F. Jing<sup>34</sup>, N. Kalantar-Nayestanaki<sup>21</sup>, M. Kavatsyuk<sup>21</sup>, W. Kuehn<sup>36</sup>, W. Lai<sup>1</sup>, J. S. Lange<sup>36</sup>, C. H. Li<sup>1</sup>, Cheng Li<sup>40</sup>, Cui Li<sup>40</sup>, D. M. Li<sup>46</sup>, F. Li<sup>1</sup>, G. Li<sup>1</sup>, H. B. Li<sup>1</sup>, J. C. Li<sup>1</sup>, K. Li<sup>10</sup>, Lei Li<sup>1</sup>, Q. J. Li<sup>1</sup>, S. L. Li<sup>1</sup>, W. D. Li<sup>1</sup>, W. G. Li<sup>1</sup>, X. L. Li<sup>29</sup>, X. N. Li<sup>1</sup>, X. Q. Li<sup>26</sup>, X. R. Li<sup>28</sup>, Z. B. Li<sup>33</sup>, H. Liang<sup>40</sup>, Y. F. Liang<sup>31</sup>, Y. T. Liang<sup>36</sup>, G. R. Liao<sup>34</sup>, X. T. Liao<sup>1</sup>, B. J. Liu<sup>1</sup>, C. L. Liu<sup>3</sup>, C. X. Liu<sup>1</sup>, C. Y. Liu<sup>1</sup>, F. H. Liu<sup>30</sup>, Fang Liu<sup>1</sup>, Feng Liu<sup>15</sup>, H. Liu<sup>1</sup>, H. H. Liu<sup>13</sup>, H. M. Liu<sup>1</sup>, H. W. Liu<sup>1</sup>, J. P. Liu<sup>44</sup>, K. Y. Liu<sup>23</sup>, Kai Liu<sup>6</sup>, P. L. Liu<sup>29</sup>, Q. Liu<sup>6</sup>, S. B. Liu<sup>40</sup>, X. Liu<sup>22</sup>, Y. B. Liu<sup>26</sup>, Z. A. Liu<sup>1</sup>, Zhiqiang Liu<sup>1</sup>, Zhiqing Liu<sup>1</sup>, H. Loehner<sup>21</sup>, G. R. Lu<sup>12</sup>, H. J. Lu<sup>14</sup>, J. G. Lu<sup>1</sup>, Q. W. Lu<sup>30</sup>, X. R. Lu<sup>6</sup>, Y. P. Lu<sup>1</sup>, C. L. Luo<sup>24</sup>, M. X. Luo<sup>45</sup>, T. Luo<sup>37</sup>, X. L. Luo<sup>1</sup>, M. Lv<sup>1</sup>, C. L. Ma<sup>6</sup>, F. C. Ma<sup>23</sup>, H. L. Ma<sup>1</sup>, Q. M. Ma<sup>1</sup>, S. Ma<sup>1</sup>, T. Ma<sup>1</sup>, X. Y. Ma<sup>1</sup>, Y. Ma<sup>11</sup>, F. E. Maas<sup>11</sup>, M. Maggiora<sup>43A,43C</sup>, Q. A. Malik<sup>42</sup>, Y. J. Mao<sup>27</sup>, Z. P. Mao<sup>1</sup>, J. G. Messchendorp<sup>21</sup>, J. Min<sup>1</sup>, T. J. Min<sup>1</sup>, R. E. Mitchell<sup>17</sup>, X. H. Mo<sup>1</sup>, C. Morales Morales<sup>11</sup>, C. Motzko<sup>2</sup>, N. Yu. Muchnoi<sup>5</sup>, H. Muramatsu<sup>39</sup>, Y. Nefedov<sup>20</sup>, C. Nicholson<sup>6</sup>, I. B. Nikolaev<sup>5</sup>, Z. Ning<sup>1</sup>, S. L. Olsen<sup>28</sup>, Q. Ouyang<sup>1</sup>, S. Pacetti<sup>18B</sup>, J. W. Park<sup>28</sup>, M. Pelizaeus<sup>37</sup>, H. P. Peng<sup>40</sup>, K. Peters<sup>7</sup>, J. L. Ping<sup>24</sup>, R. G. Ping<sup>1</sup>, R. Poling<sup>38</sup>, E. Prencipe<sup>19</sup>, M. Qi<sup>25</sup>, S. Qian<sup>1</sup>, C. F. Qiao<sup>6</sup>, X. S. Qin<sup>1</sup>, Y. Qin<sup>27</sup>, Z. H. Qin<sup>1</sup>, J. F. Qiu<sup>1</sup>, K. H. Rashid<sup>42</sup>, G. Rong<sup>1</sup>, X. D. Ruan<sup>9</sup>, A. Sarantsev<sup>20,d</sup>, B. D. Schaefer<sup>17</sup>, J. Schulze<sup>2</sup>, M. Shao<sup>40</sup>, C. P. Shen<sup>37,e</sup>, X. Y. Shen<sup>1</sup>, H. Y. Sheng<sup>1</sup>, M. R. Shepherd<sup>17</sup>, X. Y. Song<sup>1</sup>, S. Spataro<sup>43A,43C</sup>, B. Spruck<sup>36</sup>, D. H. Sun<sup>1</sup>, G. X. Sun<sup>1</sup>, J. F. Sun<sup>12</sup>, S. S. Sun<sup>1</sup>, Y. J. Sun<sup>40</sup>, Y. Z. Sun<sup>1</sup>, Z. J. Sun<sup>1</sup>, Z. T. Sun<sup>40</sup>, C. J. Tang<sup>31</sup>, X. Tang<sup>1</sup>, I. Tapan<sup>35C</sup>, E. H. Thorndike<sup>39</sup>, D. Toth<sup>38</sup>, M. Ullrich<sup>36</sup>, G. S. Varner<sup>37</sup>, B. Wang<sup>9</sup>, B. Q. Wang<sup>27</sup>, K. Wang<sup>1</sup>, L. L. Wang<sup>1</sup>, L. S. Wang<sup>1</sup>, M. Wang<sup>29</sup>, P. Wang<sup>1</sup>, P. L. Wang<sup>1</sup>, Q. Wang<sup>1</sup>, Q. J. Wang<sup>1</sup>, S. G. Wang<sup>27</sup>, X. L. Wang<sup>40</sup>, Y. D. Wang<sup>40</sup>, Y. F. Wang<sup>1</sup>, Y. Q. Wang<sup>29</sup>, Z. Wang<sup>1</sup>, Z. G. Wang<sup>1</sup>, Z. Y. Wang<sup>1</sup>, D. H. Wei<sup>8</sup>, P. Weidenkaff<sup>19</sup>, Q. G. Wen<sup>40</sup>, S. P. Wen<sup>1</sup>, M. Werner<sup>36</sup>, U. Wiedner<sup>2</sup>, L. H. Wu<sup>1</sup>, N. Wu<sup>1</sup>, S. X. Wu<sup>40</sup>, W. Wu<sup>26</sup>, Z. Wu<sup>1</sup>, L. G. Xia<sup>34</sup>, Z. J. Xiao<sup>24</sup>, Y. G. Xie<sup>1</sup>, Q. L. Xiu<sup>1</sup>, G. F. Xu<sup>1</sup>, G. M. Xu<sup>27</sup>, H. Xu<sup>1</sup>, Q. J. Xu<sup>10</sup>, X. P. Xu<sup>32</sup>, Z. R. Xu<sup>40</sup>, F. Xue<sup>15</sup>, Z. Xue<sup>1</sup>, L. Yan<sup>40</sup>, W. B. Yan<sup>40</sup>, Y. H. Yan<sup>16</sup>, H. X. Yang<sup>1</sup>, Y. Yang<sup>15</sup>, Y. X. Yang<sup>8</sup>, H. Ye<sup>1</sup>, M. Ye<sup>1</sup>, M. H. Ye<sup>4</sup>, B. X. Yu<sup>1</sup>, C. X. Yu<sup>26</sup>, J. S. Yu<sup>22</sup>, S. P. Yu<sup>29</sup>, C. Z. Yuan<sup>1</sup>, Y. Yuan<sup>1</sup>, A. A. Zafar<sup>42</sup>, A. Zallo<sup>18A</sup>, Y. Zeng<sup>16</sup>, B. X. Zhang<sup>1</sup>, B. Y. Zhang<sup>1</sup>, C. Zhang<sup>25</sup>, C. C. Zhang<sup>1</sup>, D. H. Zhang<sup>1</sup>, H. H. Zhang<sup>33</sup>, H. Y. Zhang<sup>1</sup>, J. Q. Zhang<sup>1</sup>, J. W. Zhang<sup>1</sup>, J. Y. Zhang<sup>1</sup>, J. Z. Zhang<sup>1</sup>, S. H. Zhang<sup>1</sup>, X. J. Zhang<sup>1</sup>, X. Y. Zhang<sup>29</sup>, Y. Zhang<sup>1</sup>, Y. H. Zhang<sup>1</sup>, Y. S. Zhang<sup>9</sup>, Z. P. Zhang<sup>40</sup>, Z. Y. Zhang<sup>44</sup>, G. Zhao<sup>1</sup>, H. S. Zhao<sup>1</sup>, J. W. Zhao<sup>1</sup>, K. X. Zhao<sup>24</sup>, Lei Zhao<sup>40</sup>, Ling Zhao<sup>1</sup>, M. G. Zhao<sup>26</sup>, Q. Zhao<sup>1</sup>, Q. Z. Zhao<sup>9,f</sup>, S. J. Zhao<sup>46</sup>, T. C. Zhao<sup>1</sup>, X. H. Zhao<sup>25</sup>, Y. B. Zhao<sup>1</sup>, Z. G. Zhao<sup>40</sup>, A. Zhemchugov<sup>20,a</sup>, B. Zheng<sup>41</sup>, J. P. Zheng<sup>1</sup>, Y. H. Zheng<sup>6</sup>, B. Zhong<sup>1</sup>, J. Zhong<sup>2</sup>, Z. Zhong<sup>9,f</sup>, L. Zhou<sup>1</sup>, X. K. Zhou<sup>6</sup>, X. R. Zhou<sup>40</sup>, C. Zhu<sup>1</sup>, K. Zhu<sup>1</sup>, K. J. Zhu<sup>1</sup>, S. H. Zhu<sup>1</sup>, X. L. Zhu<sup>34</sup>, Y. C. Zhu<sup>40</sup>, Y. M. Zhu<sup>26</sup>, Y. S. Zhu<sup>1</sup>, Z. A. Zhu<sup>1</sup>, J. Zhuang<sup>1</sup>, B. S. Zou<sup>1</sup>, J. H. Zou<sup>1</sup>

(BESIII Collaboration)

<sup>1</sup> Institute of High Energy Physics, Beijing 100049, P. R. China<sup>2</sup> Bochum Ruhr-University, 44780 Bochum, Germany<sup>3</sup> Carnegie Mellon University, Pittsburgh, PA 15213, USA<sup>4</sup> China Center of Advanced Science and Technology, Beijing 100190, P. R. China<sup>5</sup> G.I. Budker Institute of Nuclear Physics SB RAS (BINP), Novosibirsk 630090, Russia<sup>6</sup> Graduate University of Chinese Academy of Sciences, Beijing 100049, P. R. China<sup>7</sup> GSI Helmholtzcentre for Heavy Ion Research GmbH, D-64291 Darmstadt, Germany<sup>8</sup> Guangxi Normal University, Guilin 541004, P. R. China<sup>9</sup> Guangxi University, Nanning 530004, P. R. China<sup>10</sup> Hangzhou Normal University, Hangzhou 310036, P. R. China<sup>11</sup> Helmholtz Institute Mainz, J.J. Becherweg 45, D 55099 Mainz, Germany<sup>12</sup> Henan Normal University, Xinxiang 453007, P. R. China<sup>13</sup> Henan University of Science and Technology, Luoyang 471003, P. R. China<sup>14</sup> Huangshan College, Huangshan 245000, P. R. China<sup>15</sup> Huazhong Normal University, Wuhan 430079, P. R. China<sup>16</sup> Hunan University, Changsha 410082, P. R. China<sup>17</sup> Indiana University, Bloomington, Indiana 47405, USA<sup>18</sup> (A)INFN Laboratori Nazionali di Frascati, Frascati, Italy; (B)INFN and University of Perugia, I-06100, Perugia, Italy<sup>19</sup> Johannes Gutenberg University of Mainz, Johann-Joachim-Becher-Weg 45, 55099 Mainz, Germany<sup>20</sup> Joint Institute for Nuclear Research, 141980 Dubna, Russia<sup>21</sup> KVI/University of Groningen, 9747 AA Groningen, The Netherlands<sup>22</sup> Lanzhou University, Lanzhou 730000, P. R. China

- <sup>23</sup> Liaoning University, Shenyang 110036, P. R. China  
<sup>24</sup> Nanjing Normal University, Nanjing 210046, P. R. China  
<sup>25</sup> Nanjing University, Nanjing 210093, P. R. China  
<sup>26</sup> Nankai University, Tianjin 300071, P. R. China  
<sup>27</sup> Peking University, Beijing 100871, P. R. China  
<sup>28</sup> Seoul National University, Seoul, 151-747 Korea  
<sup>29</sup> Shandong University, Jinan 250100, P. R. China  
<sup>30</sup> Shanxi University, Taiyuan 030006, P. R. China  
<sup>31</sup> Sichuan University, Chengdu 610064, P. R. China  
<sup>32</sup> Soochow University, Suzhou 215006, China  
<sup>33</sup> Sun Yat-Sen University, Guangzhou 510275, P. R. China  
<sup>34</sup> Tsinghua University, Beijing 100084, P. R. China  
<sup>35</sup> (A)Ankara University, Ankara, Turkey; (B)Dogus University, Istanbul, Turkey; (C)Uludag University, Bursa, Turkey  
<sup>36</sup> Universitaet Giessen, 35392 Giessen, Germany  
<sup>37</sup> University of Hawaii, Honolulu, Hawaii 96822, USA  
<sup>38</sup> University of Minnesota, Minneapolis, MN 55455, USA  
<sup>39</sup> University of Rochester, Rochester, New York 14627, USA  
<sup>40</sup> University of Science and Technology of China, Hefei 230026, P. R. China  
<sup>41</sup> University of South China, Hengyang 421001, P. R. China  
<sup>42</sup> University of the Punjab, Lahore-54590, Pakistan  
<sup>43</sup> (A)University of Turin, Turin, Italy; (B)University of Eastern Piedmont, Alessandria, Italy; (C)INFN, Turin, Italy  
<sup>44</sup> Wuhan University, Wuhan 430072, P. R. China  
<sup>45</sup> Zhejiang University, Hangzhou 310027, P. R. China  
<sup>46</sup> Zhengzhou University, Zhengzhou 450001, P. R. China  
<sup>a</sup> also at the Moscow Institute of Physics and Technology, Moscow, Russia  
<sup>b</sup> on leave from the Bogolyubov Institute for Theoretical Physics, Kiev, Ukraine  
<sup>c</sup> Nankai University, Tianjin, 300071, China  
<sup>d</sup> also at the PNPI, Gatchina, Russia  
<sup>e</sup> now at Nagoya University, Nagoya, Japan  
<sup>f</sup> Guangxi University, Nanning, 530004, China

Using a sample of  $(225.3 \pm 2.8) \times 10^6$   $J/\psi$  decays collected with the BESIII detector at BEPCII, searches for invisible decays of  $\eta$  and  $\eta'$  in  $J/\psi \rightarrow \phi\eta$  and  $\phi\eta'$  are performed. Decays of  $\phi \rightarrow K^+K^-$  are used to tag the  $\eta$  and  $\eta'$  decays. No signals above background are found for the invisible decays, and upper limits at the 90% confidence level are determined to be  $2.58 \times 10^{-4}$  for the ratio  $\frac{\mathcal{B}(\eta \rightarrow \text{invisible})}{\mathcal{B}(\eta \rightarrow \gamma\gamma)}$  and  $2.39 \times 10^{-2}$  for  $\frac{\mathcal{B}(\eta' \rightarrow \text{invisible})}{\mathcal{B}(\eta' \rightarrow \gamma\gamma)}$ .

PACS numbers: 13.25.Gv, 13.20.Jf, 14.40.Be

## I. INTRODUCTION

Invisible decays of quarkonia to final state particles that are not observable in general purpose particle detectors offer a window into physics beyond the standard model (SM) [1–3]. This is because, aside from neutrinos, the SM includes no other invisible particles that these states can decay into. Observation of the quarkonium states coupling to invisible final states can provide information on new neutral particles such as photinos or neutralinos, very light gravitinos, or light dark matter candidates (LDM) [1–3]. These LDM particles may have the necessary density to account for the non-baryonic mass of the Universe [4].

It is in any case very interesting to search for such light invisible particles in collider experiments [5], especially since LDM is a proposed interpretation for the origin of the 511 keV line from the galactic bulge observed by the SPI spectrometer on the International Gamma-Ray Astrophysics Lab (INTEGRAL) satellite [6]. Many searches for the invisible decays of  $\pi^0$ ,  $\eta$ ,  $\eta'$ ,  $J/\psi$  and  $\Upsilon(1S)$  have

been performed by previous experiments [7–10]. Invisible  $\eta$  ( $\eta'$ ) decays may produce a pair of LDM particles in the MeV mass range, with expected rates depending on the spin and couplings of the particle mediating the decays. A spin-1  $U$  boson [11] would contribute only through its axial couplings to quarks. Invisible  $\eta$  ( $\eta'$ ) decays could also occur from  $\eta$  ( $\eta'$ )  $\rightarrow UU$ , with the  $U$  decaying invisibly into neutrinos or LDM particles [2]. For spin-0 boson exchanges tentative order of magnitude estimates for the branching fractions to a pair of LDM particles  $\mathcal{B}(\eta$  ( $\eta'$ )  $\rightarrow \chi\chi) \approx 1.4 \times 10^{-4}$  ( $1.5 \times 10^{-6}$ ) have been given in [12], using the WMAP [13] result on the relic density of the Universe.

Using  $58 \times 10^6$   $J/\psi$  events, the BESII experiment obtained a first upper limit of  $\mathcal{B}(\eta$  ( $\eta'$ )  $\rightarrow \text{invisible})/\mathcal{B}(\eta$  ( $\eta'$ )  $\rightarrow \gamma\gamma) < 1.65 \times 10^{-3}$  ( $6.69 \times 10^{-2}$ ), corresponding to an upper limit of  $\mathcal{B}(\eta$  ( $\eta'$ )  $\rightarrow \text{invisible}) < 6.5 \times 10^{-4}$  ( $1.5 \times 10^{-3}$ ) [8]. Complementary to the BESII results, IceCube set  $\mathcal{B}(\eta \rightarrow \nu_e, \tau \bar{\nu}_e, \tau) < 6.1 \times 10^{-4}$  [14] for  $\eta$  decays into SM neutrinos.

In this paper, we present updated results of searches

for the invisible decays of  $\eta$  and  $\eta'$ . The data sample used consists of  $(225.3 \pm 2.8) \times 10^6$   $J/\psi$  events [15] collected with the BESIII detector [16] at the BEPCII collider [17].

## II. THE BESIII EXPERIMENT AND MONTE CARLO SIMULATION

BEPCII/BESIII [16] is a major upgrade of the BESII experiment at the BEPC accelerator. The design peak luminosity of the double-ring  $e^+e^-$  collider, BEPCII, is  $10^{33} \text{ cm}^{-2} \text{ s}^{-1}$  at a beam current of 0.93 A. The BESIII detector has a geometrical acceptance of 93% of  $4\pi$  and consists of four main components: (1) a small-celled, helium-based main draft chamber (MDC) with 43 layers, which provides measurements of ionization energy loss ( $dE/dx$ ). The average single wire resolution is  $135 \mu\text{m}$ , and the momentum resolution for charged particles with momenta of 1 GeV/c in a 1 T magnetic field is 0.5%; (2) an electromagnetic calorimeter (EMC) made of 6240 CsI (Tl) crystals arranged in a cylindrical shape (barrel) plus two end-caps. For 1.0 GeV photons, the energy resolution is 2.5% in the barrel and 5% in the end-caps, and the position resolution is 6 mm in the barrel and 9 mm in the end-caps; (3) a time-of-flight system (TOF) for particle identification (PID) composed of a barrel part made of two layers with 88 pieces of 5 cm thick, 2.4 m long plastic scintillators in each layer, and two end-caps with 96 fan-shaped, 5 cm thick, plastic scintillators in each end-cap. The time resolution is 80 ps in the barrel, and 110 ps in the end-caps, corresponding to a  $2\sigma$   $K/\pi$  separation for momenta up to about 1.0 GeV/c; (4) a muon chamber system made of 1000  $\text{m}^2$  of resistive-plate-chambers arranged in 9 layers in the barrel and 8 layers in the end-caps and incorporated in the return iron of the super-conducting magnet. The position resolution is about 2 cm.

The optimization of the event selection and the estimation of physics backgrounds are performed using Monte Carlo (MC) simulated data samples. The GEANT4-based simulation software BOOST [18] includes the geometric and material description of the BESIII detectors, the detector response and digitization models, as well as the tracking of the detector running conditions and performance. The production of the  $J/\psi$  resonance is simulated by the MC event generator KKMC [19]; the known decay modes are generated by EVTGEN [20] with branching ratios set at PDG values [21], while the remaining unknown decay modes are modeled by LUNDCHARM [22].

## III. DATA ANALYSIS

### A. Analyses for $\eta$ and $\eta' \rightarrow$ invisible

In order to detect invisible  $\eta$  and  $\eta'$  decays, we use  $J/\psi \rightarrow \phi\eta$  and  $\phi\eta'$ . These two-body decays provide a very simple event topology, in which the  $\phi$  candidates can

be reconstructed easily and cleanly decaying into  $K^+K^-$ . The reconstructed  $\phi$  particles can be used to tag  $\eta$  and  $\eta'$  in order to allow a search for their invisible decays. In addition, both the  $\phi$  and  $\eta(\eta')$  are given strong boosts in the  $J/\psi$  decay, so the directions of the  $\eta$  and  $\eta'$  decays are well defined in the lab system and any decay products can be efficiently detected by the BESIII detector. The missing  $\eta$  and  $\eta'$  can be searched for in the distribution of mass recoiling against the  $\phi$  candidate.

Charged tracks in the BESIII detector are reconstructed using track-induced signals in the MDC. We select tracks that originate within  $\pm 10$  cm of the interaction point (IP) in the beam direction and within 1 cm in the plane perpendicular to the beam. The tracks must be within the MDC fiducial volume,  $|\cos\theta| < 0.93$  ( $\theta$  is the polar angle with respect to the  $e^+$  beam direction). Candidate events are required to have only two charged tracks reconstructed with a net charge of zero. For each charged track, information from TOF and  $dE/dx$  are combined to calculate  $\chi^2_{\text{PID}}(i)$  values. With the corresponding number of degree of freedom, we obtain probabilities,  $\text{Prob}_{\text{PID}}(i)$ , for the hypotheses that a track is a pion, kaon, or proton, where  $i$  ( $i = \pi/K/p$ ) is the particle type. For both kaon candidates, we require  $\text{Prob}_{\text{PID}}(K) > \text{Prob}_{\text{PID}}(\pi)$ . The mass recoiling against the  $\phi$  candidate,  $M_{\phi}^{\text{recoil}}$ , is calculated using the four-momentum of the incident beams in the lab frame ( $p_{\text{lab}}^{\mu} = p_{e^-}^{\mu} + p_{e^+}^{\mu}$ ), and constructing the 4-product  $(M_{\phi}^{\text{recoil}})^2 = (p_{\text{lab}} - p_{KK})^{\mu}(p_{\text{lab}} - p_{KK})_{\mu}$ , where  $p_{KK}^{\mu} = p_{\phi}^{\mu}$  is the sum of the four-momentum of the two charged kaons. The  $\eta$  and  $\eta'$  signal regions in the  $M_{\phi}^{\text{recoil}}$  distribution are defined to be within  $3\sigma$  of the known masses of  $\eta$  and  $\eta'$  [21]. Here,  $\sigma$  is the detector resolution and is 17.8 (9.3) MeV/c<sup>2</sup>, which is determined from MC simulation, for  $J/\psi \rightarrow \phi\eta(\eta')$ .

Electromagnetic showers are reconstructed from clusters of energy deposits in the EMC crystals. The shower energies are required to be greater than 25 MeV for the barrel region ( $|\cos\theta| < 0.8$ ) and 50 MeV for the end-cap region ( $0.86 < |\cos\theta| < 0.92$ ). The showers in the transition region between barrel and end-cap are required to have an energy greater than 100 MeV. Showers must be isolated from all charged tracks by more than  $10^\circ$ .

We require that  $\eta(\eta') \rightarrow$  invisible events have no charged tracks besides those of the  $\phi \rightarrow K^+K^-$  candidate. In addition, the number of EMC showers ( $N_{\text{shower}}$ ), that could be from a  $K_L$  or a photon, are required to be zero inside a cone of 1.0 rad around the recoil direction against the  $\phi$  candidate. This requirement rejects most  $\eta$  and  $\eta'$  decays into visible final states. It also eliminate most backgrounds from multibody decays of  $J/\psi \rightarrow \phi + \text{anything}$ . In order to ensure that  $\eta$  and  $\eta'$  decay particles are inside the fiducial volume of the detector, the recoil direction against the  $\phi$  is required to be within the region  $|\cos\theta_{\text{recoil}}| < 0.7$ , where  $\theta_{\text{recoil}}$  is the polar angle of the recoil three-momentum of  $\phi$  candidate. Figure 1 (a) shows the  $K^+K^-$  invariant mass distribution after the above selection. A clear  $\phi$  peak

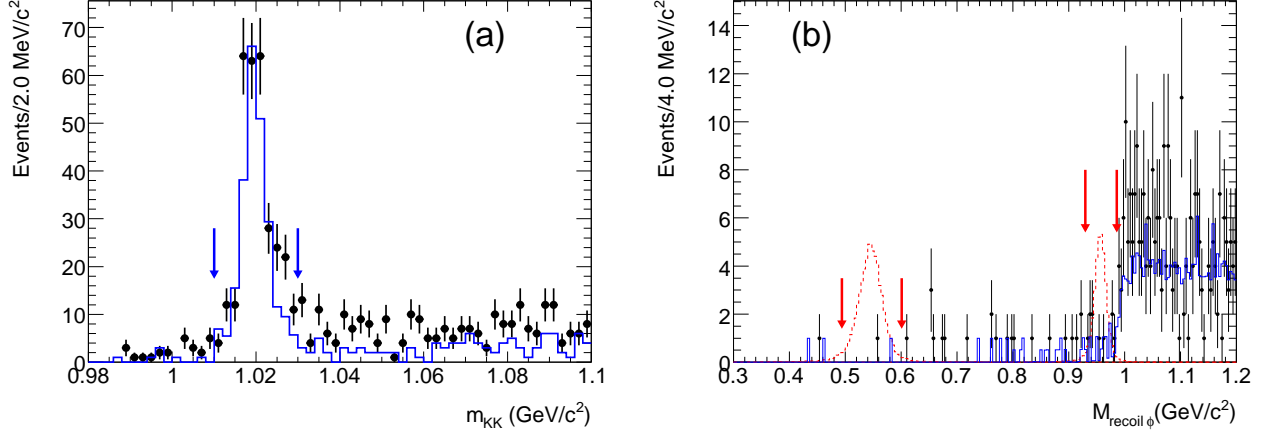


FIG. 1: (a) The  $m_{KK}$  distribution for candidate events in data. The arrows on the plot indicate the signal region of  $\phi$  candidates. Points with error bars are data; the (blue) histogram is expected background. (b) Recoil mass distribution against  $\phi$  candidates,  $M_{\phi}^{\text{recoil}}$ , for events with  $1.01 \text{ GeV}/c^2 < m_{KK} < 1.03 \text{ GeV}/c^2$  in (a). Points with error bars are data; the (blue) solid histogram is the sum of the expected backgrounds; the dashed histograms (with arbitrary scale) are signals of  $\eta$  and  $\eta'$  invisible decays from MC simulations; the arrows on the plot indicate the signal regions of the  $\eta$  and  $\eta' \rightarrow \text{invisible}$ .

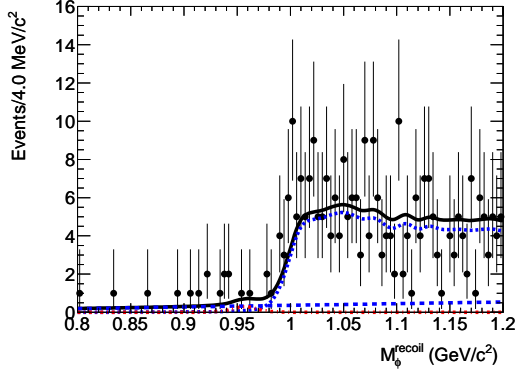


FIG. 2: The  $M_{\phi}^{\text{recoil}}$  distribution with events around the  $\eta'$  mass region. Points with error bars are data. The (black) solid curve shows the result of the fit to signal plus background distributions, the (blue) dotted curve shows the background shape from  $J/\psi \rightarrow \phi f_0(980) (f_0(980) \rightarrow K_L K_L)$ , the (blue) dashed curve shows the polynomial function for  $J/\psi \rightarrow \phi K_L K_L$  background, and the (red) dotted-dash curve shows the signal yield.

is seen. Figure 1 (b) shows the recoil mass against  $\phi$  candidates for events with  $1.01 \text{ GeV}/c^2 < m_{KK} < 1.03 \text{ GeV}/c^2$ , and there are no significant signals in the  $\eta$  and  $\eta'$  mass regions.

We use MC simulated events to determine selection efficiencies for the signal channels and study possible backgrounds. The efficiencies are 36.0% and 36.1% for  $\eta$  and  $\eta'$  invisible decays, respectively. More than 20 exclusive decay modes are generated with full MC simulations in order to better understand the backgrounds. The sources of backgrounds are divided into two classes.

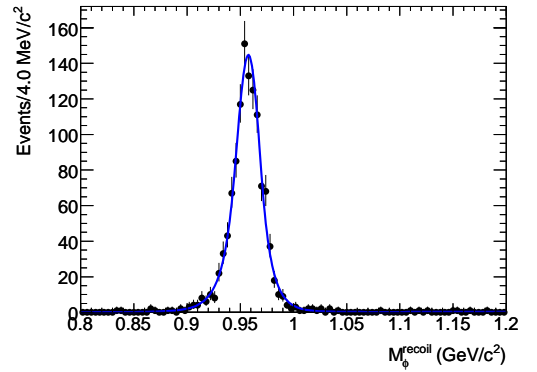


FIG. 3: The  $M_{\phi}^{\text{recoil}}$  distribution for the control sample  $J/\psi \rightarrow \phi \eta'$ ,  $\eta' \rightarrow \pi^+ \pi^- \eta (\eta \rightarrow \gamma \gamma)$  decay candidates. The solid curve shows the fit results.

Class I: The background is from  $J/\psi \rightarrow \phi \eta(\eta')$ , where  $\phi \rightarrow K^+ K^-$  and  $\eta(\eta')$  decays into visible final states that are not detected by the EMC. The expected number of background events from this class is  $0.18 \pm 0.02$  ( $1.0 \pm 0.2$ ) in the signal region for the  $\eta(\eta')$  case. Class II: It is from  $J/\psi$  decays to final states without  $\eta(\eta')$  or without both  $\eta(\eta')$  and  $\phi$ . For the  $\eta$  invisible decay, the dominant background is from  $J/\psi \rightarrow \gamma \eta_c$ ,  $\eta_c \rightarrow K^\pm \pi^\mp K_L$ , while for the  $\eta'$  case, the dominant background is from  $J/\psi \rightarrow \phi K_L K_L$  and  $J/\psi \rightarrow \phi f_0(980)$ ,  $f_0(980) \rightarrow K_L K_L$ . The expected number of background events from class II is  $0.8 \pm 0.2$  and  $9.4 \pm 1.7$  in the signal regions for  $\eta$  and  $\eta'$ , respectively.

After all selection criteria are applied, only one event (shown in Fig. 1 (b)) survives in the  $\eta$  signal region where  $1.0 \pm 0.2$  background event is expected. An upper limit (UL) at the 90% confidence level (C.L.) of  $N_{\text{UL}}^\eta = 3.34$  for

$J/\psi \rightarrow \phi\eta$  ( $\phi \rightarrow K^+K^-$  and  $\eta \rightarrow$  invisible) is obtained using the POLE<sup>++</sup> program [23] with the Feldman-Cousins frequentist approach [24]. The information used to obtain the upper limit includes the number of observed events in the signal region, and the expected number of background events and their uncertainty.

For the  $\eta'$  case, an unbinned extended maximum likelihood (ML) fit to the  $M_\phi^{\text{recoil}}$  distribution in the range  $0.8 \text{ GeV}/c^2 < M_\phi^{\text{recoil}} < 1.2 \text{ GeV}/c^2$ , as shown in Fig. 2, is performed. The signal shape used in the fit, shown in Fig. 3, is obtained from a nearly background-free  $J/\psi \rightarrow \phi\eta'$ ,  $\eta' \rightarrow \pi^+\pi^-\eta$ ,  $\eta \rightarrow \gamma\gamma$  sample. The purity of the sample is greater than 98.5%. The shape of the invisible signal peak in the  $M_\phi^{\text{recoil}}$  distribution is fixed to the smoothed histograms of the  $J/\psi \rightarrow \phi\eta'$ ,  $\eta' \rightarrow \pi^+\pi^-\eta$ ,  $\eta \rightarrow \gamma\gamma$  MC sample, and the signal yield is allowed to float. The shape of the dominant background  $J/\psi \rightarrow \phi f_0(980)$ ,  $f_0(980) \rightarrow K_L K_L$  is described by MC simulated data, in which the  $f_0(980)$  line shape is parameterized with the Flatté form [25]

$$f(m) = \frac{1}{M_{f_0}^2 + m^2 + i(g_1^2 \rho_{\pi\pi} + g_2^2 \rho_{KK})}, \quad (1)$$

where  $M_{f_0}$  is the mass of the  $f_0(980)$ ,  $m$  is the effective mass,  $\rho$  is Lorentz invariant phase space ( $\rho = 2k/m$ , here,  $k$  refers to the  $\pi$  or  $K$  momentum in the rest frame of the resonance), and  $g_1$  and  $g_2$  are coupling-constants for the  $f_0(980)$  resonance coupling to the  $\pi\pi$  and  $KK$  channels, respectively. These parameters [ $M_{f_0} = 0.965 \pm 0.010 \text{ GeV}/c^2$ ,  $g_1^2 = 0.165 \pm 0.018 (\text{GeV}/c^2)^2$  and  $g_2^2 = 0.695 \pm 0.075 (\text{GeV}/c^2)^2$ ] have been determined in the analysis of  $J/\psi \rightarrow \phi\pi^+\pi^-$  and  $\phi K^+K^-$  from BESII data [26, 27]. In the ML fit, the dominant background shape ( $J/\psi \rightarrow \phi f_0(980)$ ,  $f_0(980) \rightarrow K_L K_L$ ) is fixed to the MC simulations, and its yield ( $N_{f_0}^{\text{bkg}}$ ) is floated. The shape of the remaining background from  $J/\psi \rightarrow \phi K_L K_L$  is modeled with a first order Chebychev polynomial whose slope and yield ( $N_{\text{non-}f_0}^{\text{bkg}}$ ) are floated in the fit to data. The signal yield,  $N_{\text{sig}}^{\eta'} = 2.3 \pm 4.3$ , is consistent with zero observed events, and the resulting fitted values of  $N_{f_0}^{\text{bkg}}$  and  $N_{\text{non-}f_0}^{\text{bkg}}$  are  $239 \pm 28$  and  $37 \pm 25$ , respectively, where the errors are statistical. We obtain an upper limit by integrating the normalized likelihood distribution over the positive values of the number of signal events. The upper limit at the 90% C.L. is  $N_{UL}^{\eta'} = 10.1$ .

### B. Analyses for $\eta$ and $\eta' \rightarrow \gamma\gamma$

The branching fraction of  $\eta(\eta') \rightarrow \gamma\gamma$  is also determined in  $J/\psi \rightarrow \phi\eta(\eta')$ , in order to obtain the ratio of  $\mathcal{B}(\eta(\eta') \rightarrow \text{invisible})$  to  $\mathcal{B}(\eta(\eta') \rightarrow \gamma\gamma)$ . The advantage of measuring  $\frac{\mathcal{B}(\eta(\eta') \rightarrow \text{invisible})}{\mathcal{B}(\eta(\eta') \rightarrow \gamma\gamma)}$  is that the uncertainties due to the total number of  $J/\psi$  events, tracking efficiency, PID, the number of the charged tracks, and the residual noise in the EMC cancel.

The selection criteria for the charged tracks are the same as those for  $J/\psi \rightarrow \phi\eta(\eta')$ ,  $\eta(\eta') \rightarrow$  invisible. However, at least two good photons are required. The events are kinematically fitted using energy and momentum conservation constraints (4C) under the  $J/\psi \rightarrow KK\gamma\gamma$  hypothesis in order to obtain better mass resolution and suppress backgrounds further. We require the kinematic fit  $\chi_{K^+K^-\gamma\gamma}^2$  to be less than 90 (40) for the  $\eta(\eta')$  case. If there are more than two photons, the fit is repeated using all permutations, and the combination with the best fit to  $KK\gamma\gamma$  is retained.

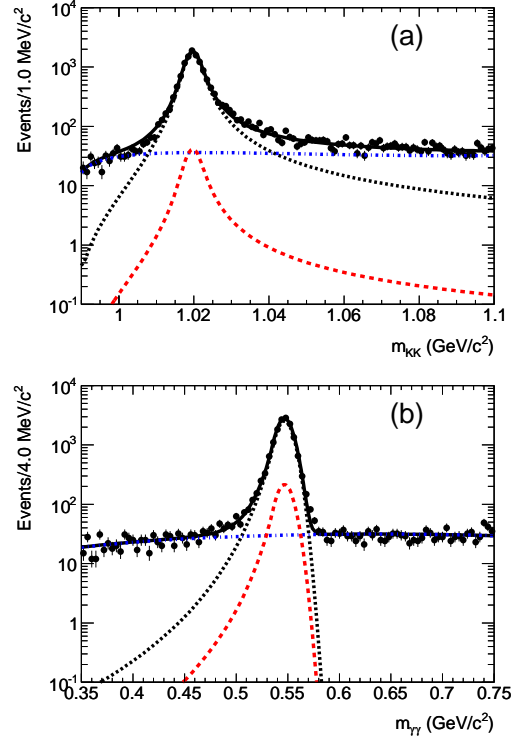


FIG. 4: The (a)  $m_{KK}$  and (b)  $m_{\gamma\gamma}$  distributions with fit results superimposed for  $J/\psi \rightarrow \phi\eta$ ,  $\phi \rightarrow K^+K^-$ ,  $\eta \rightarrow \gamma\gamma$ . Points with error bars are data. The (black) solid curves show the results of the fits to signal plus background, and the (black) dashed curves are for signal. In (a), the (blue) dotted-dash curve shows non- $\phi$ -peaking backgrounds, and the (red) short-dashed curve shows the non- $\eta$ -peaking background. In (b), the (blue) dotted-dash curve shows non- $\eta$ -peaking backgrounds, and the (red) short-dashed curve shows the non- $\phi$ -peaking background.

The numbers of  $J/\psi \rightarrow \phi\eta(\eta')$ ,  $\eta(\eta') \rightarrow \gamma\gamma$  events are obtained from an extended unbinned ML fit to the  $K^+K^-$  versus  $\gamma\gamma$  invariant mass distributions. The projection of the fit on the  $m_{KK}$  ( $m_{\gamma\gamma}$ ) axis is shown in Figs. 4(a) and 5(a) (Figs. 4(b) and 5(b)) for the  $\eta$  and  $\eta'$  cases, respectively. In the ML fits, we require that  $0.99 \text{ GeV}/c^2 < m_{KK} < 1.10 \text{ GeV}/c^2$  and  $0.35 \text{ GeV}/c^2 < m_{\gamma\gamma} < 0.75 \text{ GeV}/c^2$  ( $0.75 \text{ GeV}/c^2 < m_{\gamma\gamma} < 1.15 \text{ GeV}/c^2$ ) for the  $\eta(\eta')$  case. The signal shape for  $\phi$  is

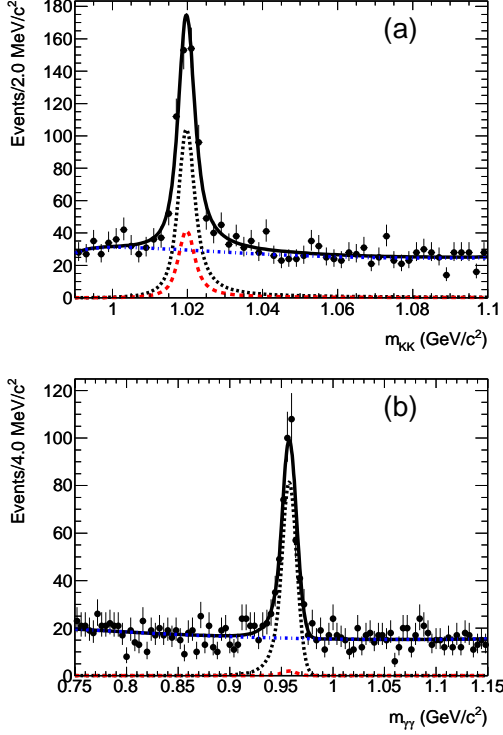


FIG. 5: The (a)  $m_{KK}$  and (b)  $m_{\gamma\gamma}$  distributions with fit results superimposed for  $J/\psi \rightarrow \phi\eta'$ ,  $\phi \rightarrow K^+K^-$ ,  $\eta' \rightarrow \gamma\gamma$ . Points with error bars are data. The (black) solid curves show the results of the fits to signal plus background distributions, and the (black) dashed curves are for signal. In (a), the (blue) dotted-dash curve shows non- $\phi$ -peaking backgrounds, and the (red) short-dashed curve shows the non- $\eta'$ -peaking background. In (b), the (blue) dotted-dash curve shows non- $\eta'$ -peaking backgrounds, and the (red) short-dashed curve shows the non- $\phi$ -peaking background.

modeled with a relativistic Breit-Wigner ( $RBW$ ) function [28] convoluted with a Gaussian function that represents the detector resolution; the signal shape for  $\eta(\eta')$  is described by a Crystal Ball ( $CB$ ) function [29], and its parameters are floated. In the ML fits, the width of  $\phi$  is fixed at the PDG value, and its central mass value is floated. The backgrounds are divided into three categories: non- $\phi(\eta')$ -peaking background (*i.e.*,  $J/\psi \rightarrow \gamma\pi^0 K^+K^-$ , in which one of the photons is missing); non- $\phi$ -peaking background (*i.e.*,  $J/\psi \rightarrow K^+K^-\eta(\eta')$ ); and non- $\eta(\eta')$ -peaking background (*i.e.*,  $J/\psi \rightarrow \phi\gamma\gamma$  and  $\phi\pi^0\pi^0$ ). The probability density functions (PDF) for non- $\phi$ -peaking background in the  $m_{KK}$  distribution is parameterized by [30]

$$B(m_{KK}) = (m_{KK} - 2m_K)^a \cdot e^{-bm_{KK} - cm_{KK}^2}, \quad (2)$$

where  $a$ ,  $b$  and  $c$  are free parameters, and  $m_K$  is the nominal mass value of the charged kaon from the PDG [21]. The shape for the non- $\eta(\eta')$ -peaking background in the  $m_{\gamma\gamma}$  distribution is modeled by a second-order Cheby-

chev polynomial function ( $B(m_{\gamma\gamma})$ ). All parameters related to the background shape are floated in the fit to data. The PDFs for signal and backgrounds are combined in the likelihood function  $\mathcal{L}$ , defined as a function of the free parameters  $N_{\gamma\gamma}^\eta$ ,  $N_{\text{bkg}}^{\text{non-}\phi\eta}$ ,  $N_{\text{bkg}}^{\text{non-}\phi}$ , and  $N_{\text{bkg}}^{\text{non-}\eta}$ :

$$\begin{aligned} \mathcal{L} = & \frac{e^{-(N_{\gamma\gamma}^\eta + N_{\text{bkg}}^{\text{non-}\phi\eta} + N_{\text{bkg}}^{\text{non-}\phi} + N_{\text{bkg}}^{\text{non-}\eta})}}{N!} \\ & \times \prod_{i=1}^N [N_{\gamma\gamma}^\eta RBW(m_{KK}^i) \times CB(m_{\gamma\gamma}^i) \\ & + N_{\text{bkg}}^{\text{non-}\phi\eta} B(m_{KK}^i) \times B(m_{\gamma\gamma}^i) \\ & + N_{\text{bkg}}^{\text{non-}\phi} B(m_{KK}^i) \times CB(m_{\gamma\gamma}^i) \\ & + N_{\text{bkg}}^{\text{non-}\eta} RBW(m_{KK}^i) \times B(m_{\gamma\gamma}^i)], \quad (3) \end{aligned}$$

where  $N_{\gamma\gamma}^\eta$  is the number of  $J/\psi \rightarrow \phi\eta$ ,  $\phi \rightarrow K^+K^-$ ,  $\eta \rightarrow \gamma\gamma$  events, and  $N_{\text{bkg}}^{\text{non-}\phi\eta}$ ,  $N_{\text{bkg}}^{\text{non-}\phi}$ , and  $N_{\text{bkg}}^{\text{non-}\eta}$  are the numbers of the corresponding three kinds of backgrounds. The fixed parameter  $N$  is the total number of selected events in the fit region, and  $m_{KK}^i$  ( $m_{\gamma\gamma}^i$ ) is the value of  $m_{KK}$  ( $m_{\gamma\gamma}$ ) for the  $i$ th event. We use the product of the PDFs, since we have verified that  $m_{KK}$  and  $m_{\gamma\gamma}$  are uncorrelated for each component. The negative log-likelihood ( $-\ln\mathcal{L}$ ) is then minimized with respect to the extracted yields. The resulting fitted signal and background yields are summarized in Table I. We also obtain the results for the  $\eta'$  case by replacing  $\eta$  with  $\eta'$  in Eq. (3). The fitted results for  $\eta(\eta') \rightarrow \gamma\gamma$  are shown in Fig. 4 (Fig. 5). The detection efficiencies are determined with MC simulations to be 36.3% and 31.7% for  $\eta$  and  $\eta'$ , respectively.

TABLE I: The fitted signal and background yields for  $J/\psi \rightarrow \phi\eta(\eta')$ ,  $\eta(\eta') \rightarrow \gamma\gamma$ , and  $\epsilon_{\gamma\gamma}^\eta$  ( $\epsilon_{\gamma\gamma}^{\eta'}$ ) is its selection efficiency.

Quantity	Value	
	$\eta$	$\eta'$
$N_{\gamma\gamma}^\eta$ ( $N_{\gamma\gamma}^{\eta'}$ )	$13390 \pm 136$	$400 \pm 25$
$N_{\text{bkg}}^{\text{non-}\phi\eta}$ ( $N_{\text{bkg}}^{\text{non-}\phi\eta'}$ )	$2514 \pm 64$	$1482 \pm 46$
$N_{\text{bkg}}^{\text{non-}\phi}$ ( $N_{\text{bkg}}^{\text{non-}\phi}$ )	$1132 \pm 70$	$10 \pm 15$
$N_{\text{bkg}}^{\text{non-}\eta}$ ( $N_{\text{bkg}}^{\text{non-}\eta'}$ )	$313 \pm 54$	$159 \pm 26$
$\epsilon_{\gamma\gamma}^\eta$ ( $\epsilon_{\gamma\gamma}^{\eta'}$ )	36.3%	31.7%

According to the results in Table I, the ratio of  $\mathcal{B}(J/\psi \rightarrow \phi\eta)$  to  $\mathcal{B}(J/\psi \rightarrow \phi\eta')$ , is found to be consistent with the known value [21]. The individual branching fraction is larger by  $1.3(1.6)\sigma$  with respect to the average value listed in Ref. [21] for  $\mathcal{B}(J/\psi \rightarrow \phi\eta(\eta'))$ , while it is consistent with Ref. [8].

#### IV. SYSTEMATIC UNCERTAINTIES

The contributions to the systematic error on the calculation of the ratios are summarized in Table II. The uncertainty, due to the requirement of no neutral showers in the EMC inside the 1.0 rad cones around the recoil direction against the  $\phi$  candidate, is estimated using the control sample of fully reconstructed  $J/\psi \rightarrow \phi\eta$ ,  $\eta \rightarrow \gamma\gamma$  events. The ratios of events with no extra photons to events without this requirement are obtained for both data and MC simulation. The difference 0.3% is taken as the systematic error for both the  $\eta$  and  $\eta'$  cases. This study determines the difference of the noise in the EMC for MC simulation and data. The uncertainty due to the  $\phi$  mass window requirement is determined to be 1.5% by using the same control sample of  $J/\psi \rightarrow \phi\eta$ ,  $\eta \rightarrow \gamma\gamma$  events.

For the  $\eta'$  invisible decay, systematic errors in the ML fit originate from the limited number of events in the data sample and from uncertainties in the PDF parameterizations. Since the signal shape is obtained from the  $J/\psi \rightarrow \phi\eta'$ ,  $\eta' \rightarrow \pi^+\pi^-\eta$ ,  $\eta \rightarrow \gamma\gamma$  events in the data, the uncertainty due to the signal shape is negligible. The uncertainty due to the background shape is estimated by varying the PDF shape of the background in the ML fit. The shape of the dominant background  $J/\psi \rightarrow \phi f_0(980)$ ,  $f_0(980) \rightarrow K_L K_L$  is parameterized with the Flatté form in Eq. (1). To estimate the uncertainty, we change the central values of the parameters used in the fit by one standard deviation of the measured values [26], and find that the relative error on  $\eta' \rightarrow$  invisible decay is 1.0%. The systematic uncertainty due to the choice of parameterization for the shape of the background from  $J/\psi \rightarrow \phi K_L K_L$  is estimated by varying the order of the polynomial in the fit; we find a relative change on the invisible signal yield of 2.9%, which is taken as the uncertainty due to the background model.

The uncertainty in the determination of the number of observed  $J/\psi \rightarrow \phi\eta(\eta')$ ,  $\phi \rightarrow K^+K^-$ ,  $\eta(\eta') \rightarrow \gamma\gamma$  events is also estimated. The systematic error due to photon detection is determined to be 1% for each photon [31]. The uncertainty due to the 4C fit is estimated to be 0.4%(0.8%) for the  $\eta(\eta')$  case using the control sample  $J/\psi \rightarrow \pi^0 K^+K^-$ . In the fit to the  $\phi$  mass distribution, the mass resolution is fixed to the MC simulation; the level of possible discrepancy is determined with a smearing Gaussian, for which a non-zero  $\sigma$  would represent a MC-data difference in the mass resolution. The uncertainty associated with a difference determined in this way is 0.1% (1.0%) for the  $\eta(\eta')$  case. The systematic uncertainty due to the choice of parameterization for the shape of the non- $\phi\eta(\eta')$ -peaking background is estimated by varying the order of the polynomial in the fit; we find the relative changes on the  $\eta(\eta')$  signal yield of 0.1% (0.6%), which is taken as the uncertainty due to the background shapes. The total systematic errors  $\sigma_{\eta}^{\text{sys}}$  and  $\sigma_{\eta'}^{\text{sys}}$  on the ratio are 2.5% and 4.1% for  $\eta$  and  $\eta'$ , as

summarized in Table II.

TABLE II: Summary of errors. The first four lines are relative systematic errors for  $J/\psi \rightarrow \phi\eta(\eta')$ ,  $\eta(\eta') \rightarrow$  invisible. The next four lines are relative systematic errors for  $J/\psi \rightarrow \phi\eta(\eta')$ ,  $\eta(\eta') \rightarrow \gamma\gamma$ . The second line from the bottom is the relative statistical error of  $N_{\gamma\gamma}^{\eta}(N_{\gamma\gamma}^{\eta'})$ .

Source of uncertainties	Sys. error (%)	
	$\eta$	$\eta'$
Requirement on $N_{\text{shower}}$	0.3	0.3
$\phi$ mass window	1.5	1.5
Background shape of $J/\psi \rightarrow \phi f_0(980)$	-	1.0
Background shape of $J/\psi \rightarrow \phi K_L K_L$	-	2.9
4C fit for $\eta(\eta') \rightarrow \gamma\gamma$	0.4	0.8
Photon detection	2.0	2.0
Signal shapes for $\eta(\eta') \rightarrow \gamma\gamma$	0.1	1.0
Background shape for $\eta(\eta') \rightarrow \gamma\gamma$	0.1	0.6
Total systematic errors	2.5	4.1
Statistical error of $N_{\gamma\gamma}^{\eta}(N_{\gamma\gamma}^{\eta'})$	1.0	6.0
Total errors	2.7	7.4

#### V. RESULTS

The upper limit at the 90% confidence level on the ratio of  $\mathcal{B}(\eta \rightarrow \text{invisible})$  to  $\mathcal{B}(\eta \rightarrow \gamma\gamma)$  is calculated with

$$\frac{\mathcal{B}(\eta \rightarrow \text{invisible})}{\mathcal{B}(\eta \rightarrow \gamma\gamma)} < \frac{N_{UL}^{\eta}/\epsilon_{\eta}}{N_{\gamma\gamma}^{\eta}/\epsilon_{\gamma\gamma}} \frac{1}{1 - \sigma_{\eta}}, \quad (4)$$

where  $N_{UL}^{\eta}$  is the 90% upper limit of the number of observed events for  $J/\psi \rightarrow \phi\eta$ ,  $\phi \rightarrow K^+K^-$ ,  $\eta \rightarrow$  invisible decay,  $\epsilon_{\eta}$  is the MC determined efficiency for the signal channel,  $N_{\gamma\gamma}^{\eta}$  is the number of events for the  $J/\psi \rightarrow \phi\eta$ ,  $\phi \rightarrow K^+K^-$ ,  $\eta \rightarrow \gamma\gamma$ ,  $\epsilon_{\gamma\gamma}^{\eta}$  is the MC determined efficiency, and  $\sigma_{\eta}$  is the total error for the  $\eta$  case from Table II. The upper limit on the ratio of  $\mathcal{B}(\eta' \rightarrow \text{invisible})$  to  $\mathcal{B}(\eta' \rightarrow \gamma\gamma)$  is obtained similarly.

Thus, the upper limit of  $2.58 \times 10^{-4}$  ( $2.39 \times 10^{-2}$ ) on the ratio of  $\mathcal{B}(\eta(\eta') \rightarrow \text{invisible})$  and  $\mathcal{B}(\eta(\eta') \rightarrow \gamma\gamma)$  is obtained at the 90% confidence level.

#### VI. CONCLUSION

In summary, the invisible decays of  $\eta$  and  $\eta'$  are searched for in the two-body decays  $J/\psi \rightarrow \phi\eta$  and  $\phi\eta'$  using  $(225.3 \pm 2.8) \times 10^6$   $J/\psi$  decays collected with the BESIII detector. We find no signal above background for the invisible decays of  $\eta$  and  $\eta'$  and obtain upper limits at the 90% C.L. of  $2.58 \times 10^{-4}$  and  $2.39 \times 10^{-2}$



for  $\frac{\mathcal{B}(\eta \rightarrow \text{invisible})}{\mathcal{B}(\eta \rightarrow \gamma\gamma)}$  and  $\frac{\mathcal{B}(\eta' \rightarrow \text{invisible})}{\mathcal{B}(\eta' \rightarrow \gamma\gamma)}$ , respectively. Using the branching fraction values of  $\eta$  and  $\eta' \rightarrow \gamma\gamma$  from the PDG [21], we determine the invisible decay rates to be  $\mathcal{B}(\eta \rightarrow \text{invisible}) < 1.0 \times 10^{-4}$  and  $\mathcal{B}(\eta' \rightarrow \text{invisible}) < 5.3 \times 10^{-4}$  at the 90% confidence level.

Our limits are improved by factors of 6 and 3 compared to the previous ones obtained at BESII [8], the  $\eta'$  limit being almost 2 times better than the recent one from the CLEO-c experiment [32]. The limit for  $\eta \rightarrow \text{invisible}$  is smaller than a possible estimate [12] for the  $\eta \rightarrow \chi\chi$  decay to a pair of MeV dark matter particles, no such decays, however, being expected for a spin-1  $U$  mediator with vector couplings to quarks (or axial ones in the limit of small  $m_\chi$ ). These limits constrain the decays  $\eta(\eta') \rightarrow UU$  with each  $U$  decaying invisibly (into neutrinos or LDM), with branching fraction  $B_{\text{inv}}$ . The resulting  $\eta(\eta')$  limits on the  $U$  couplings to quarks are improved by  $\simeq 1.6$  and  $1.3$  as compared to those obtained in [2] from the BESII limits [8], and now read  $\sqrt{f_u^2 + f_d^2} < 3 \cdot 10^{-2}/\sqrt{B_{\text{inv}}}$  and  $|f_s| < 4 \cdot 10^{-2}/\sqrt{B_{\text{inv}}}$ , respectively, where  $f_u$ ,  $f_d$  and  $f_s$  are effective couplings of  $U$  boson to light quarks [2].

### Acknowledgments

The BESIII collaboration thanks the staff of BEPCII and the computing center for their hard efforts. One

of the authors, Hai-Bo Li, thank Pierre Fayet for illuminating suggestions. This work is supported in part by the Ministry of Science and Technology of China under Contract No. 2009CB825200; National Natural Science Foundation of China (NSFC) under Contracts Nos. 10625524, 10821063, 10825524, 10835001, 10935007, 11125525; Joint Funds of the National Natural Science Foundation of China under Contracts Nos. 11079008, 11179007, 11179014; the Chinese Academy of Sciences (CAS) Large-Scale Scientific Facility Program; CAS under Contracts Nos. KJCX2-YW-N29, KJCX2-YW-N45; 100 Talents Program of CAS; Istituto Nazionale di Fisica Nucleare, Italy; Ministry of Development of Turkey under Contract No. DPT2006K-120470; U. S. Department of Energy under Contracts Nos. DE-FG02-04ER41291, DE-FG02-91ER40682, DE-FG02-94ER40823; U.S. National Science Foundation; University of Groningen (RuG) and the Helmholtzzentrum fuer Schwerionenforschung GmbH (GSI), Darmstadt; WCU Program of National Research Foundation of Korea under Contract No. R32-2008-000-10155-0.

- 
- [1] P. Fayet, Phys. Lett. B **84**, 421 (1979); P. Fayet and J. Kaplan, Phys. Lett. B **269**, 213 (1991); B. McElrath, Phys. Rev. D **72**, 103508 (2005).
  - [2] P. Fayet, Phys. Rev. D **74**, 054034 (2006).
  - [3] P. Fayet, Phys. Rev. D **75**, 115017 (2007); P. Fayet, Phys. Lett. B **675**, 267 (2009); P. Fayet, Phys. Rev. D **81**, 054025 (2010).
  - [4] C. Boehm, D. Hooper, J. Silk, M. Casse, and J. Paul, Phys. Rev. Lett. **92**, 101301 (2004); J. F. Beacom, N. F. Bell, and G. Bertone, Phys. Rev. Lett. **94**, 171301 (2005); N. Borodatchenkova, D. Choudhury, and M. Drees, Phys. Rev. Lett. **96**, 141802 (2006).
  - [5] H. B. Li and T. Luo, Phys. Lett. B **686**, 249 (2010).
  - [6] P. Jean *et al.*, Astron. Astrophys. **407**, L55 (2003); SPI is the spectrometer aboard INTEGRAL.
  - [7] A. V. Artamonov *et al.* (E949 Collaboration), Phys. Rev. D **72**, 091102 (2005).
  - [8] M. Ablikim *et al.* (BES Collaboration), Phys. Rev. Lett. **97**, 202002 (2006).
  - [9] M. Ablikim *et al.* (BES Collaboration), Phys. Rev. Lett. **100**, 192001 (2008).
  - [10] B. Aubert *et al.* (BABAR Collaboration), Phys. Rev. Lett. **103**, 251801 (2009); P. Rubin *et al.* (CLEO Collaboration), Phys. Rev. D **75**, 031104 (2007); O. Tajima *et al.* (Belle Collaboration), Phys. Rev. Lett. **98**, 132001 (2007); R. Balest *et al.* (CLEO Collaboration), Phys. Rev. D **51**, 2053 (1995).
  - [11] P. Fayet, Nucl. Phys. B **187**, 184 (1981).
  - [12] B. McElrath, arXiv:0712.0016[hep-ph], *Proceedings of the CHARM 2007 Workshop*, Ithaca, NY, August 5-8, 2007.
  - [13] D. N. Spergel *et al.* (WMAP Collaboration), Astrophys. J. Suppl. Ser. **148**, 175 (2003).
  - [14] A. R. Fazely *et al.*, Phys. Rev. D **81**, 117101 (2010).
  - [15] M. Ablikim *et al.* (BESIII Collaboration), arXiv:1207.2865, accepted for publication by Chinese Physics C.
  - [16] M. Ablikim *et al.* (BESIII Collaboration), Nucl. Instrum. Meth. A **614**, 345 (2010).
  - [17] D. M. Asner *et al.*, Int. J. Mod. Phys. A **24**, Suppl. (2009).
  - [18] S. Agostinelli *et al.* (GEANT4 Collaboration), Nucl. Instrum. Meth. A **506**, 250 (2003).
  - [19] S. Jadach, B. F. L. Ward and Z. Was, Comput. Phys. Commun. **130**, 260 (2000); S. Jadach, B. F. L. Ward and Z. Was Phys. Rev. D **63**, 113009 (2001).
  - [20] D. J. Lange, Nucl. Instrum. Meth. A **462**, 152 (2001).
  - [21] J. Beringer *et al.* (Particle Data Group), Phys. Rev. D **86**, 010001 (2012).
  - [22] J. C. Chen, G. S. Huang, X. R. Qi, D. H. Zhang, and Y. S. Zhu, Phys. Rev. D **62**, 034003 (2000).
  - [23] J. Conrad, O. Botner, A. Hallgren and C. Pérez de los Heros, Phys. Rev. D **67**, 012002 (2003); <http://polepp.googlecode.com/svn/tags/POLEPP-1.1.0>.
  - [24] G. J. Feldman and R. D. Cousins, Phys. Rev. D **57**, 3873 (1998).
  - [25] S. M. Flatté, Phys. Lett. B **63**, 224 (1976).
  - [26] M. Ablikim *et al.* (BES Collaboration), Phys. Lett. B



- 607**, 243 (2005).
- [27] It is noted that different definition of Flatté form is used in Eq. (1) in Ref. [26]. Here,  $g_1^2$  and  $g_2^2$  are identical to ‘ $g_1$ ’ and ‘ $g_2$ ’ in Ref. [26]. Therefore, we notice that the unit for the ‘ $g_1$ ’ and ‘ $g_2$ ’ in Ref. [26] should be  $(\text{GeV}/c^2)^2$  instead of  $\text{GeV}/c^2$ .
  - [28] F. von Hippel and C. Quigg, Phys. Rev. D **5**, 624, (1972); J. Blatt and V. Weisskopf, *Theoretical Nuclear Physics*, New York: John Wiley & Sons (1952).
  - [29] J. E. Gaiser, Ph. D. Thesis, SLAC-R-255 (1982) (unpublished); M. J. Oreglia, Ph. D. Thesis, SLAC-R-236 (1980) (unpublished); T. Skwarnicki, Ph. D. Thesis, DESY-F-31-86-02 (1986) (unpublished).
  - [30] C. C. Chang *et al.* (E580 Collaboration), Phys. Rev. D **29**, 1888 (1984); D. Barberis *et al.* (WA102 Collaboration), Phys. Lett. B **436**, 204 (1998).
  - [31] M. Ablikim *et al.* (BESIII Collaboration), Phys. Rev. D **83**, 112005 (2011).
  - [32] P. Naik *et al.* (CLEO Collaboration), Phys. Rev. Lett. **102**, 061801 (2009).